J. Fluid Mech. (1969), *vol.* 36, *part* 3, *pp.* 529–543
Printed in Great Britain

Fluctuating turbulent stresses in the noise-producing region of a jet

By IAN S. F. JONES†
Department of Mechanical Engineering, University of Waterloo, Waterloo, Ontario

(Received 14 May 1968)

Measurements of the fluctuating turbulent stresses $(u_i u_j)'$ in the mixing layer of a two-dimensional jet are presented. These include the intensity, spatial correlation and the wave-number frequency spectra of the fluctuating stresses.

The acoustic spectrum perpendicular to the axis of a jet can be approximated with the aid of assumptions about jet similarity and a knowledge of the four-dimensional wave-number frequency spectrum at zero wave-number. In the present paper the four-dimensional spectrum was inferred from measured two-dimensional spectra and the self-noise spectrum perpendicular to a round jet estimated. Good agreement was obtained with measured acoustic spectra.

1. Introduction

Lighthill (1952) has connected the acoustic density fluctuations ρ' to the stress field for a region of turbulence. For an observer at $\mathbf{x}$ in a medium with a density ρ_0 and with a speed of sound a_0, the acoustic density fluctuations are

$$\rho'(\mathbf{x}) = \frac{x_i x_j}{4\pi a_0^4 |\mathbf{x}|^3} \int \frac{\partial^2}{\partial t^2} \rho_0 v_i v_j (\mathbf{y}, \tau)\, d\mathbf{y}, \tag{1.1}$$

where τ is retarded time and the volume integration is performed over all space.

The expression for the acoustic density can be expanded by writing for the velocity v_i its mean and fluctuating components $U_i + u_i$ and by manipulating (1.1) with the aid of the equations of motion (for example, see Jones (1968), amongst others). The resultant expression, which contains shear-noise terms and self-noise terms, is

$$\rho'(\mathbf{x}) = \frac{x_i x_j}{4\pi a_0^4 |\mathbf{x}|^3} \int \left[2 \frac{\partial U_j}{\partial y_k} \frac{\partial}{\partial t} (\rho_0 u_i u_k + p \delta_{ik}) + \frac{\partial^2}{\partial t^2} \rho_0 u_i u_j \right] (\mathbf{y}, \tau)\, d\mathbf{y}, \tag{1.2}$$

where we have neglected some terms involving higher-order derivatives of $\partial U_i / \partial y_k$.

In order to provide a better understanding of the acoustic radiation from a jet, a series of measurements of the stresses has been made. Because the time differentiation in (1.2) eliminates the mean part of the stress, only the fluctuations about the mean were considered. The jets studied differed from many previous jets investigated in that the mixing layers sprang from a nozzle with turbulent

† Present address: Department of Mechanical Engineering, University of Sydney.

boundary layers. This situation was studied as it was felt to more closely resemble the most important practical source of aerodynamic noise, the aircraft turbine engine.

2. Apparatus

The instantaneous velocities were sensed by 0·0002 in. diameter platinum plated tungsten wires, 0·04 in. long, heated by DISA 55A01 constant current anemometers. The signal processing was done with the aid of Philbrick operational amplifiers, the overall frequency response (-3 db) extending from 0·4 c/s to 15 kc. Care was taken to see that all components had a peak to r.m.s. capability

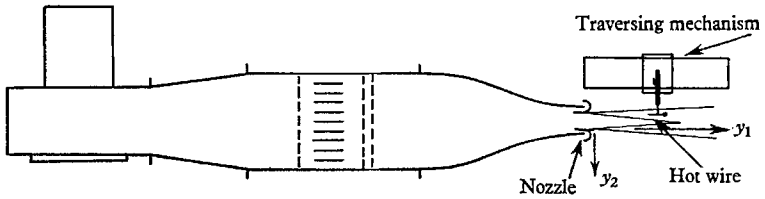

FIGURE 1. Wind tunnel with nozzle no. 2 showing co-ordinates used.

Nozzle no. 2	
Size	18 in. × 4 in.
Exit velocity	$U_0 = 113$ ft./sec
Free stream turbulence	$\sqrt{u_1^2}/U_0 = 0{\cdot}0015$
Wall boundary layer	$\delta_{0.995} = 0{\cdot}10$ in.
Momentum thickness	$\theta = 0{\cdot}013$ in.
Shear stress coefficient	$c_f = 0{\cdot}0050$

TABLE 1. Nozzle data.

of 10:1. The time averaging was performed by passing the signal through a voltage-to-frequency converter and counting the number of pulses over periods up to 100 sec. A Bruel and Kjaer 2112 spectrum analyzer was used to measure the spectra while the filtered correlations were obtained with the aid of two-phase locked Hewlett Packard 302A wave analyzers.

The measurements in this study were made downstream of a two-dimensional nozzle which was designated nozzle 2. This exit had slightly convergent walls arranged so that the boundary layers were bled off 5 in. upstream of the exit. The air was supplied by a fixed speed 3 h.p. centrifugal fan, the arrangement being shown in figure 1. The exit conditions of the nozzle are listed in table 1.

3. Velocities

The mean velocity profile across the jet is shown in figure 2 for the downstream position $y_1 = 10$ in. (i.e. 2·5 exit widths).

The intensity of the velocity fluctuations, shown in figure 3, exhibits a marked

departure from the results of Bradshaw, Ferriss & Johnson (1964). In Bradshaw's round jet, exit diameter 2 in., the maximum values of $\sqrt{u_1^2}/U_0$ and $\sqrt{u_3^2}/U_0$ were much the same while the maximum value of $\sqrt{u_2^2}/U_0$ was about 7% less than the former pair. The present results with smaller values of $\sqrt{u_2^2}/U_0$ compared with

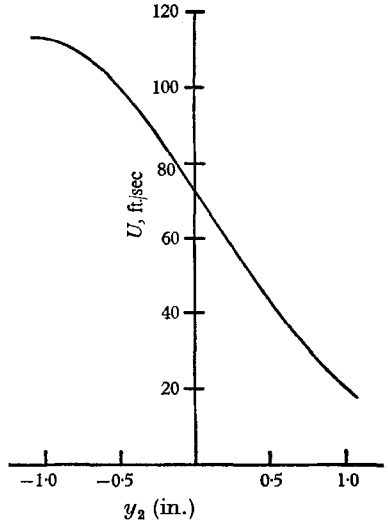

FIGURE 2. Mean velocity profile. Nozzle no. 2, $y_1 = 10$ in.

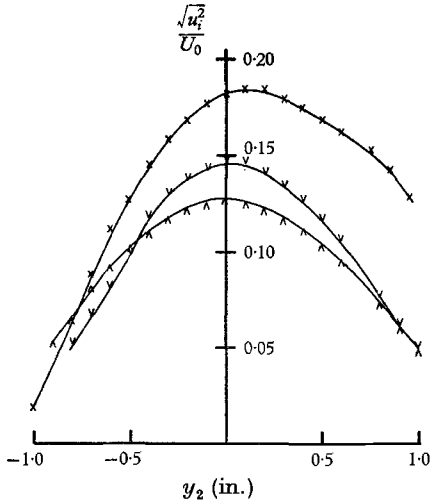

FIGURE 3. Turbulent velocities. Nozzle no. 2, $y_1 = 10$ in., $U_0 = 113$ ft./sec. ×, $\sqrt{u_1^2}/U_0$; ∧, $\sqrt{u_2^2}/U_0$; ∨, $\sqrt{u_3^2}/U_0$.

$\sqrt{u_1^2}/U_0$ are more in agreement with the measurements of Liepmann & Laufer (1947) on a two-dimensional jet. Measurements within the first diameter downstream of an 8 in. diameter round jet also showed a marked difference between the lateral and longitudinal intensities. This evidence leads one to suggest that the radius of curvature may be important in determining the relative magnitude of the maximum intensities.

The maximum intensity of $\sqrt{\overline{u_1^2}}/U_0$ at a number of cross-sections is plotted against distance downstream in figure 4. In the boundary layer on the nozzle walls, the maximum value of the root mean square of the longitudinal velocity fluctuations divided by the square root of wall shear stress,

$$\sqrt{\overline{u_1^2}}/\sqrt{\tau_w} = 2{\cdot}0$$

is a little below that measured by Laufer (1955) in the inner layer of a pipe.

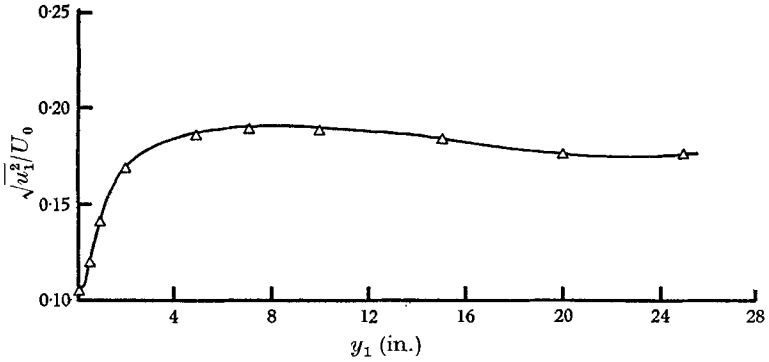

FIGURE 4. Maximum turbulent intensities at a cross-section. Nozzle no. 2.

The maximum turbulent intensities measured are rather higher than measured values for nozzles with laminar boundary layers (Bradshaw *et al.* (1964) measured a maximum intensity 0·14). Lower values of intensity have been measured by the author on nozzles with lower wall shear stress.

4. Intensity of stress fluctuations

The turbulent Reynolds stresses, divided by density, can be written as the product of the turbulent velocities u_i and u_j. We will denote the fluctuations of this product about its mean as

$$(u_i u_j)' = u_i u_j - \overline{u_i u_j}$$

and the intensity of the stress fluctuations relative to the nozzle exit velocity, U_0, as

$$\frac{\overline{(u_i u_j)'(u_l u_m)'}}{U_0^4}.$$

While this intensity represents in general 21 terms, in the two-dimensional situation the terms containing odd powers of u_3 vanish and so there are only 13 possible non-zero products. These products are listed in table 2.

Products with interchanged indices can be related to each other by expanding the product of the total stresses from the fluctuating velocities into their mean and fluctuating components. One can write

$$\begin{aligned}\overline{u_i u_j u_l u_m} &= \overline{[(u_i u_j)' + \overline{u_i u_j}][(u_l u_m)' + \overline{u_l u_m}]} \\ &= \overline{(u_i u_j)'(u_l u_m)'} + \overline{u_i u_j}\,\overline{u_l u_m}\end{aligned}$$

or

$$\overline{u_i u_l u_j u_m} = \overline{(u_i u_l)'(u_j u_m)'} + \overline{u_i u_l}\,\overline{u_j u_m}.$$

Stress	Max value U_0^4	Velocity	Max value U_0^2	Velocity	Max value U_0^2	Correlation	Correlation value
$\overline{u_1^{2\prime}u_1^{2\prime}}$	0·0021	$\overline{u_1^2}$	0·0343	$\overline{u_1^2}$	0·0343	$\overline{u_2^{2\prime}u_1^{2\prime}}/\overline{u_1^2}\,\overline{u_1^2}$	1·8
$\overline{u_2^{2\prime}u_2^{2\prime}}$	0·0005	$\overline{u_2^2}$	0·0161	$\overline{u_2^2}$	0·0161	$\overline{u_2^{2\prime}u_2^{2\prime}}/\overline{u_2^2}\,\overline{u_2^2}$	1·9
$\overline{u_3^{2\prime}u_3^{2\prime}}$	0·00093	$\overline{u_3^2}$	0·021	$\overline{u_3^2}$	0·021	$\overline{u_3^{2\prime}u_3^{2\prime}}/\overline{u_3^2}\,\overline{u_3^2}$	2·1
$\overline{(u_1u_2)'^2}$	0·00075	$\overline{u_1^2}$	0·0343	$\overline{u_2^2}$	0·0161	$\overline{(u_1u_2)'^2}/\overline{u_1^2}\,\overline{u_2^2}$	1·35
$\overline{(u_1u_3)'^2}$	0·00075	$\overline{u_1^2}$	0·0343	$\overline{u_3^2}$	0·021	$\overline{(u_1u_3)'^2}/\overline{u_1^2}\,\overline{u_3^2}$	1·05
$\overline{(u_2u_3)'^2}$	0·00036	$\overline{u_2^2}$	0·0161	$\overline{u_3^2}$	0·021	$\overline{(u_2u_3)'^2}/\overline{u_2^2}\,\overline{u_3^2}$	1·07
$\overline{u_1^{2\prime}u_2^{2\prime}}$	0·00048	$\overline{u_1^2}$	0·0343	$\overline{u_2^2}$	0·0161	$\overline{u_1^{2\prime}u_2^{2\prime}}/\overline{u_1^2}\,\overline{u_2^2}$	0·87
$\overline{u_1^{2\prime}u_3^{2\prime}}$	0·0	$\overline{u_1^2}$	0·0343	$\overline{u_3^2}$	0·021	$\overline{u_1^{2\prime}u_3^{2\prime}}/\overline{u_1^2}\,\overline{u_3^2}$	0·0
$\overline{u_2^{2\prime}u_3^{2\prime}}$	0·0	$\overline{u_2^2}$	0·0161	$\overline{u_3^2}$	0·021	$\overline{u_2^{2\prime}u_3^{2\prime}}/\overline{u_2^2}\,\overline{u_3^2}$	0·0
$\overline{u_1^{2\prime}(u_1u_2)'}$	0·00075	$\sqrt{\overline{u_1^{2\prime}u_1^{2\prime}}}$	0·046	$\sqrt{\overline{(u_1u_2)'^2}}$	0·0274	$\overline{u_1^{2\prime}(u_1u_2)'}/\sqrt{\overline{u_1^{2\prime}u_1^{2\prime}}}\sqrt{\overline{(u_1u_2)'^2}}$	0·60
$\overline{u_2^{2\prime}(u_1u_2)'}$	0·0005	$\sqrt{\overline{u_2^{2\prime}u_2^{2\prime}}}$	0·0224	$\sqrt{\overline{(u_1u_2)'^2}}$	0·0274	$\overline{u_2^{2\prime}(u_1u_2)'}/\sqrt{\overline{u_2^{2\prime}u_2^{2\prime}}}\sqrt{\overline{(u_1u_2)'^2}}$	0·65

TABLE 2. Fluctuating turbulent stresses in a two-dimensional jet.

Thus products such as $\overline{(u_1u_2)'(u_1u_2)'}$ were calculated from fluctuating stress products such as $\overline{u_1^{2\prime}u_1^{2\prime}}$ and the appropriate mean stresses.

Eleven of the stresses which were either measured directly or calculated are shown in figures 5–8. The stress product $\overline{(u_2u_3)'^2}$ was measured with a four-wire arrangement in contrast with the other stresses which were measured with single

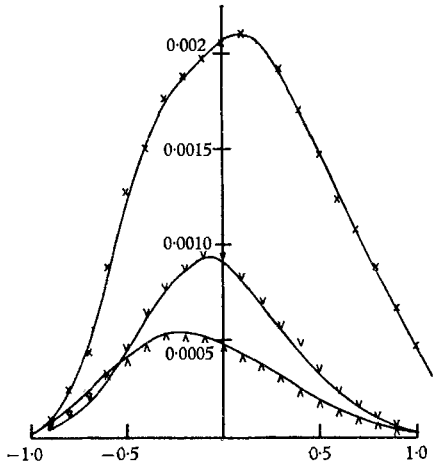

FIGURE 5

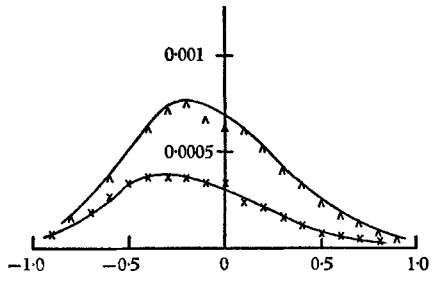

FIGURE 6

FIGURE 5. Fluctuating normal stress profiles. Nozzle no. 2, $y_1 = 10$ in., $U_0 = 113$ ft./sec. ×, $\overline{(u^{2\prime})^2}/U_0^4$; ∧, $\overline{(u_2^{2\prime})^2}/U_0^4$; ∨, $\overline{(u_3^{2\prime})^2}/U_0^4$.

FIGURE 6. Fluctuating turbulent stress profiles. Nozzle no. 2, $y_1 = 10$ in., $U_0 = 113$ ft./sec. ×, $\overline{u_2^{2\prime}(u_1u_2)'}/U_0^4$; ∧, $\overline{u_1^{2\prime}(u_1u_2)'}/U_0^4$.

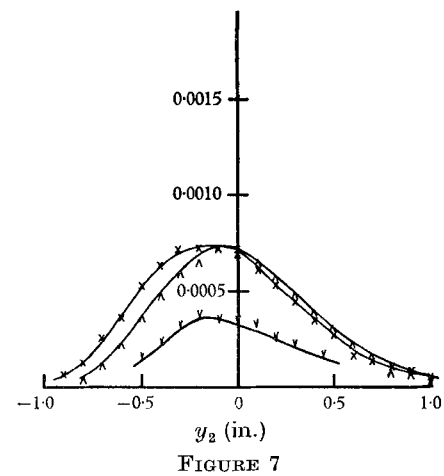

FIGURE 7

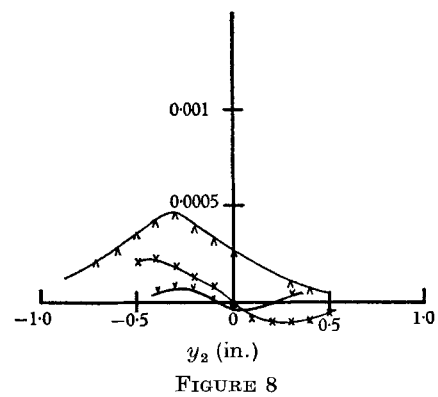

FIGURE 8

FIGURE 7. Fluctuating lateral turbulent stress profiles. Nozzle no. 2, $y_1 = 10$ in., $U_0 = 113$ ft./sec. ×, $\overline{(u_1u_2)'^2}/U_0^4$; ∧, $\overline{(u_1u_3)'^2}/U_0^4$; ∨, $\overline{(u_2u_3)'^2}/U_0^4$.

FIGURE 8. Fluctuating turbulent stress profiles. Nozzle no. 2, $y_1 = 10$ in., $U_0 = 113$ ft./sec. ×, $\overline{u_1^{2\prime}u_3^{2\prime}}/U_0^4$; ∧, $\overline{u_1^{2\prime}u_2^{2\prime}}/U_0^4$; ∨, $\overline{u_2^{2\prime}u_3^{2\prime}}/U_0^4$.

or crossed wires. The value obtained is below that measured by Bradshaw *et al.* (1964) who used only two wires.

In table 2 the maximum measured value of the mean square of stress fluctuations has been compared with the maximum values of the appropriate mean square velocity fluctuations. The stress products which are the result of two different stresses have been expressed in terms of the product of the maximum r.m.s. value of the individual stresses. This method of presentation was chosen to minimize the dependence of the stress products on the magnitude of the velocity fluctuations, i.e. $\overline{u_1^2}$, $\overline{u_2^2}$, $\overline{u_3^2}$, in any particular jet.

The mean product of the fluctuating normal stresses is related to the fourth moment of the probability distribution of the appropriate velocity by relationships such as

$$\frac{(\overline{u_1^4})}{(\overline{u_1^2})^2} - 1 = \frac{\overline{u_1^{2\prime} u_1^{2\prime}}}{(\overline{u_1^2})^2}. \tag{4.1}$$

The quantities listed in table 2 are not exactly analogous to that on the right-hand side of (4.1), since the maximum value of the stress and velocity need not occur together. The differences in the present case, however, are small. The fourth moment of the longitudinal velocity fluctuation u_1 was found to be 2·4 at $y_2 = 0$ by Davies & Fisher (1963) and the present value of 2·8 for the fourth moment, calculated from the $\overline{u_1^{2\prime} u_1^{2\prime}}$ product, is higher. Part of the difference is due to the use of non-linearized wires in the present experiment in contrast with Davies & Fisher's linearized wires. When the anemometer was linearized before squaring the fluctuating signal a 20 % reduction in the fourth moment at $y_2 = 0$ was observed. All the stresses presented will be influenced by the non-linear anemometer response.

5. Correlation coefficients

The two-point correlation coefficient of the fluctuating stresses $(u_i u_j)'$ and $(u_l u_m)'$ can be defined as

$$R_{ijlm}(\mathbf{y}, \mathbf{r}, t) = \frac{\overline{u_i u_j'(\mathbf{y}, 0) u_l u_m'(\mathbf{y}+\mathbf{r}, t)}}{\overline{u_i u_j'(\mathbf{y}, 0) u_l u_m'(\mathbf{y}, 0)}},$$

where t is time difference.

The correlation of the longitudinal normal stress was measured for separation along its three axes for zero time separation. These correlations, $R_{1111}(\mathbf{y}, r_1, 0)$, $R_{1111}(\mathbf{y}, r_2, 0)$ and $R_{1111}(\mathbf{y}, r_3, 0)$, have no negative regions along the three axes in contrast with the corresponding velocity correlation

$$R_{11}(\mathbf{y}, \mathbf{r}, 0) = \frac{\overline{u_1(\mathbf{y}, 0) u_1(\mathbf{y}+\mathbf{r}, 0)}}{\overline{u_1^2(\mathbf{y}, 0)}},$$

where continuity requires at least some regions of negative correlation. Because of the good low frequency response of the equipment used (lower -3 db point, 0·4 c/s) no correction for low frequency cut-off was made.

The three integral stress length scales, $\mathscr{L}_1$, $\mathscr{L}_2$ and $\mathscr{L}_3$ defined similarly to

$$\mathscr{L}_1(\mathbf{y}) = \int_0^\infty R_{1111}(\mathbf{y}, r_1, 0) dr_1$$

are shown along the line $y_2 = 0$ in figure 9. Also shown in this figure are the stress length scales measured at 4 diameters downstream of a circular nozzle by Chu (1966). These length scales are significantly lower than the present measurements and as well Chu reports a region of negative $R_{1111}(\mathbf{y}, r_1, 0)$ correlation. Both these differences can be attributed to the poor low frequency response (-3 db at 20 c/s) of the instruments used by Chu who discusses this point in some detail, concluding his measured length scales may be 10–20 % too low.

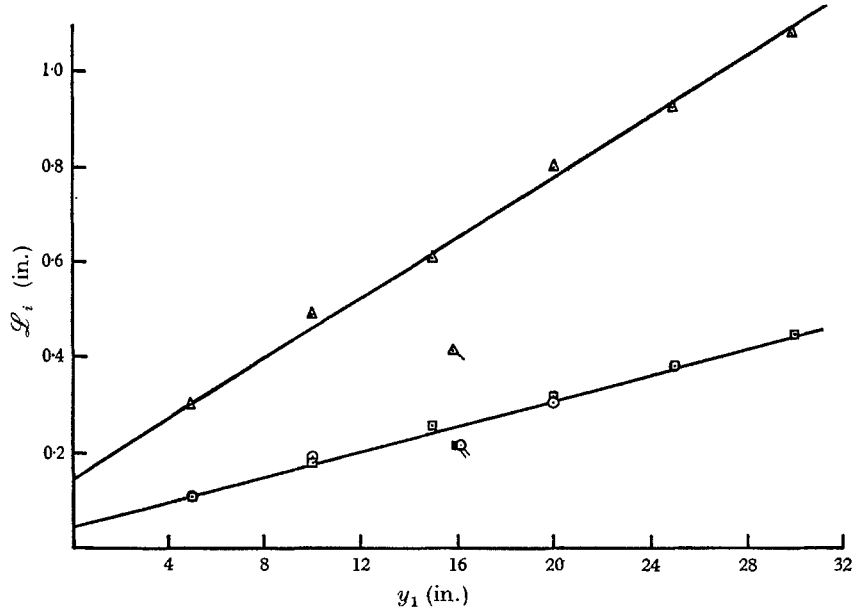

FIGURE 9. Length scale of stress along $y_2 = 0$. Nozzle no. 2, $U_0 = 113$ ft./sec: △, $\mathscr{L}_1$; □, $\mathscr{L}_2$; ○, $\mathscr{L}_3$. Chu (1966), $y_1 = 4$ diameters, $U_0 = 142$ ft./sec: △, $\mathscr{L}_1$; □, $\mathscr{L}_2$; ○, $\mathscr{L}_3$.

6. Frequency spectrum

The frequency spectrum of the fluctuating stress can be defined in terms of the auto-correlation as

$$\phi_{ijlm}(\mathbf{y}, \omega) = \left(\frac{2}{\pi}\right) \int_0^\infty R_{ijlm}(\mathbf{y}, 0, t) \cos \omega t \, dt. \tag{6.1}$$

The spectrum of the normal stress, ϕ_{1111}, and the spectrum of the velocity, ϕ_{11}, defined in a similar manner to (6.1) using $R_{11}(\mathbf{y}, 0, t)$, have been measured and are presented in figure 10 against co-ordinates normalized by the jet centre line velocity, U_{CL}, at this position. The u_1^2 fluctuations are the square of the velocity fluctuations and so the Fourier components of u_1^2 will be the result of the sum and difference of Fourier components of the velocity. Thus the spectrum of the stress fluctuations is flatter than the velocity spectrum and contains more energy at high frequencies.

7. Four-dimensional Fourier transform

A more general Fourier transform of the stress correlation, and one of particular interest in the generation of aerodynamic noise, is

$$M_{ijlm}(\mathbf{y}, \mathbf{k}, \omega) = (2/\pi)^4 \int_0^\infty \int_0^\infty R_{ijlm}(\mathbf{y}, \mathbf{r}, t) \cos \mathbf{k} \cdot \mathbf{r} \cos \omega t \, d\mathbf{r} \, dt, \tag{7.1}$$

where $M_{ijlm}(\mathbf{y}, \mathbf{k}, \omega)$ is simply related to the spectra defined over all space only in restricted cases.

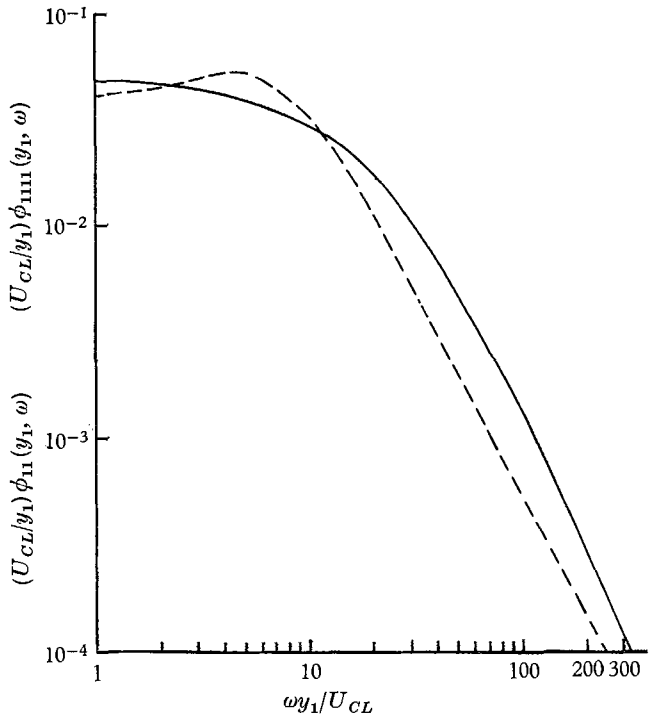

FIGURE 10. $y_1 = 10$ in., $y_2 = 0$, $U_0 = 113$ ft./sec: — — —, velocity spectrum ϕ_{11}; ——, stress spectrum ϕ_{1111}.

The spectrum of the normal stress $u_1^{2\prime}$ is determined most conveniently by the experimental technique used by Wills (1964) to obtain an analogous spectrum of the velocity fluctuations. The stress $u_1^{2\prime}$ was filtered by a narrow band filter with centre-frequency ω, at two points and these signals used to obtain the correlation $R(\omega, \mathbf{r})$ which is defined by

$$M_{1111}(\mathbf{y}, \mathbf{k}, \omega) = (2/\pi)^3 \phi_{1111}(\mathbf{y}, \omega) \int_0^\infty R(\omega, \mathbf{r}) \cos \mathbf{k}, \mathbf{r} \, d\mathbf{r}. \tag{7.2}$$

The filtered correlation has been measured at $y_2 = 0$ along the three separation axes, i.e. $R(\omega, r_1)$, $R(\omega, r_2)$ and $R(\omega, r_3)$. The correlations $R(\omega, r_2)$ and $R(\omega, r_3)$ were monotonically decreasing functions without observable negative loops, but the correlation with separations in the mean flow direction, $R(\omega, r_1)$ resembled

a damped cosine curve. Its form, shown in figure 11, resembles the filtered correlations of the fluctuating velocity measured by Wills (1964).

The filtered length scales were defined as

$$L_i^* = \int_0^\infty R(\omega, r_i)\, dr_i \quad \text{(no summation)}$$

and the lateral scales L_2^* and L_3^* measured directly from the correlations. These scales are shown in figure 12 plotted against Strouhal number

$$S = \omega y_1 / U.$$

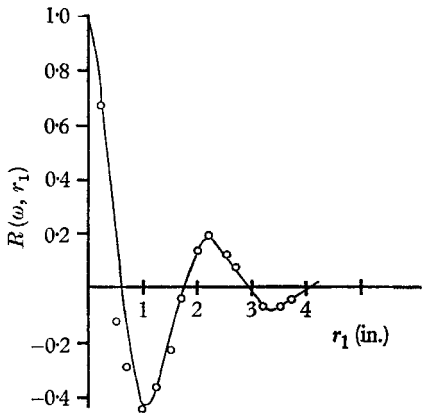

FIGURE 11

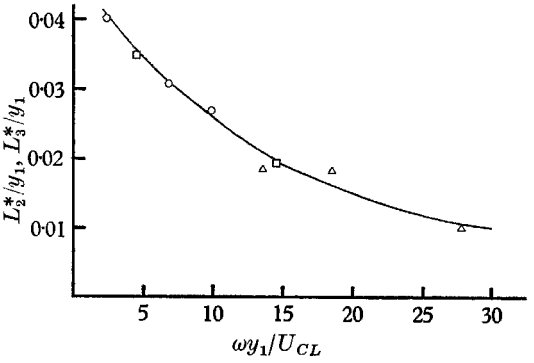

FIGURE 12

FIGURE 11. Filtered correlation coefficient. Nozzle no. 2, $y_1 = 5$ in., $y_2 = 0$, $U_0 = 113$ ft./sec, $\omega = 342$ c/s. ———, exp $-(r_1/Ay_1)$ cos $(r_1\omega/U_c)$.

FIGURE 12. Filtered length scales. Nozzle no. 2, $y_2 = 0$, $U_0 = 113$ ft./sec. ○, $y_1 = 5$ in., L_3^*; △, $y_1 = 10$ in., L_3^*; □, $y_1 = 5$ in., L_2^*.

Rather than integrate the longitudinal correlation directly, the curve

$$\exp\left[\frac{-r_1}{Ay_1}\right] \cos\frac{\omega r_1}{U_c}, \tag{7.3}$$

where U_c, a convection velocity, and A are allowed to vary, was fitted to the measured correlation. Equation (7.3) was then integrated analytically to obtain the length scale. The values of A which provided the best fit to the results are shown in figure 13 and the length scale L_1^* calculated from (7.3) is shown in figure 14.

The four-dimensional spectrum at zero wave-number follows from (7.2), i.e.

$$M_{1111}(\mathbf{y}, 0, \omega) = (2/\pi)^3 \phi_{1111}(\mathbf{y}, \omega) \int_0^\infty R(\omega, \mathbf{r})\, d\mathbf{r} \tag{7.4}$$

and can be calculated from the present measurements with the assumption that the correlation $R(\omega, \mathbf{r})$ can be separated with regard to the space variable as follows

$$R(\omega, \mathbf{r}) = R(\omega, r_1)\, R(\omega, r_2)\, R(\omega, r_3). \tag{7.5}$$

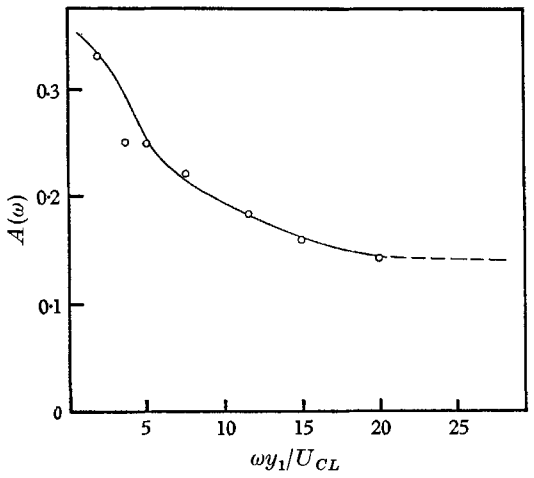

FIGURE 13

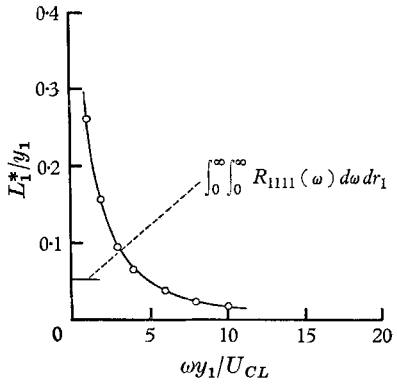

FIGURE 14

FIGURE 13. The coefficient A in the filtered correlation coefficient, $R(\omega, r_1)$. Nozzle no. 2, $y_1 = 5$ in., $y_2 = 0$, $U_0 = 113$ ft./sec.

FIGURE 14. Frequency dependent length scale. Nozzle no. 2, $y_1 = 5$ in., $y_2 = 0$, $U_0 = 113$ ft./sec.

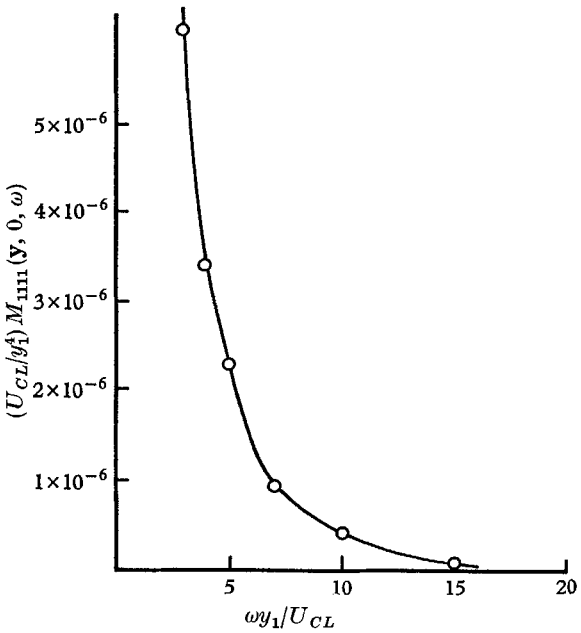

FIGURE 15. Four-dimensional stress spectrum, zero wave-number.

Notice that this assumption, that the correlation is separable in space, does not imply that it is separable in time *and* space. In fact the strong frequency dependence of the length scales in figures 12 and 14 show that separation in time and space may lead to a poor approximation for $R(\omega, \mathbf{r})$.

Using equation (7.4) and the results in figures 10, 12 and 14, the spectrum $M_{1111}(\mathbf{y}, 0, \omega)$ was calculated and is shown in figure 15 plotted against non-dimensional co-ordinates. One should remember, however that

$$\int_0^\infty \int_0^\infty M_{1111}(\mathbf{y}, \mathbf{k}, \omega) d\omega d\mathbf{k} = 1.$$

8. Acoustic spectrum

The zero wave-number spectrum of the previous section is important in aerodynamic noise because, as Ffowcs Williams (1963) has shown, the acoustic spectrum is related to the appropriate stress spectra at $\mathbf{k} = 0$. At right angles to the jet axis the expression for the acoustic radiation from a round jet is considerably simpler than the more general spectrum, so we will attempt to predict the acoustic spectrum at this position from the turbulent stress spectrum.

One can see from the expression for the acoustic fluctuations, (1.2), that the shear noise terms that radiate sound at right angles to the jet axis involve gradients of lateral velocities, i.e. $\partial U_2/\partial y_k$ and $\partial U_3/\partial y_k$. These gradients are an order of magnitude smaller than typical time scales in a round jet, since the jet spreads slowly. Thus the acoustic density fluctuations normal to the jet are generated mainly by self noise terms and can be written

$$\rho'(\mathbf{x}) = \frac{x_i x_j}{4\pi a_0^4 |\mathbf{x}|^3} \int \frac{\partial^2}{\partial t^2} \rho_0 (u_i u_j)'(\mathbf{y}, \tau) d\mathbf{y}, \tag{8.1}$$

where the time differentiation eliminates the mean part of $u_i u_j$.

Ffowcs Williams (1963) has derived the connexion between the acoustic spectrum $W(\omega)$ and his turbulence spectrum $H_{ijlm}(\mathbf{y}, \mathbf{k}, \omega)$ and we write his equation (3.9) for radiation at right angles to the jet (using a fixed frame of reference)

$$W(\omega) \sim \frac{\pi}{2\rho_0 a_0^5} \int \frac{x_i x_j x_l x_m}{|\mathbf{x}|^6} \omega^4 H_{ijlm}(\mathbf{y}, 0, -\omega) d\mathbf{y}, \tag{8.2}$$

where, if $M_{ijlm}(\mathbf{y}, 0, \omega)$ is an even function of ω,

$$H_{ijlm}(\mathbf{y}, 0, -\omega) = \rho_0^2 \overline{(u_i u_j)'(u_l u_m)'} M_{ijlm}(\mathbf{y}, 0, \omega) \quad \text{(no summation)}.$$

If we proceed to argue dimensionally we can place $\overline{(u_i u_j)'(u_l u_m)'}$ proportional to the jet centre line velocity U_{CL}^4 and $M_{ijlm}(\mathbf{y}, 0, \omega)$ proportional to $M_{1111}(\mathbf{y}, 0, \omega)$. For a self-preserving mixing layer the cross-sectional area of turbulence is an annulus of width y_1, and this area, even past the end of the uniform core, can be considered proportional to y_1. With these substitutions (8.2) can be rewritten

$$W(\omega) \sim \int_0^\infty U_{CL}^4 \omega^4 M_{1111}(\mathbf{y}, 0, \omega) y_1 dy_1. \tag{8.3}$$

The non-dimensional spectrum, $\omega^4(U_{CL}/y_1)M_{1111}(\mathbf{y}, 0, S)$ is plotted against Strouhal number $\omega y_1/U_{CL}$ in figure 16. The same spectrum computed by Chu (1966) from his measurements of correlations, using the assumption that time and lateral displacements are separable, is also shown in figure 16. Chu's spectrum peaks at significantly higher frequency and the apparent extra energy at high

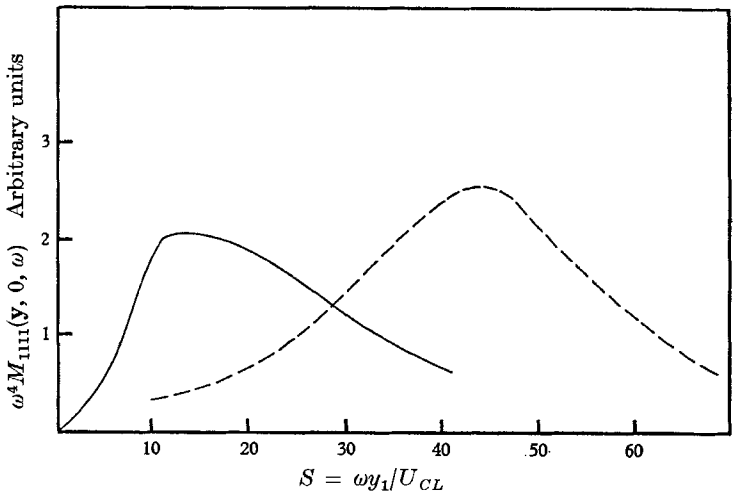

FIGURE 16. Stress spectrum: ———, present results; — — —, Chu (1966).

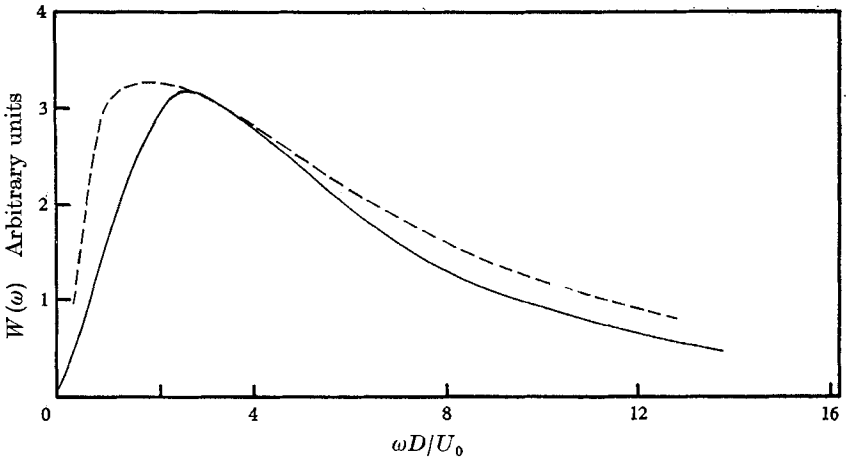

FIGURE 17. Acoustic spectrum: ———, predicted; — — —, Mollo-Christensen *et al.* (1964).

frequencies is, in part, due to the fact that Chu neglected the reduction in the region of correlation in the lateral direction of higher frequency components (as reflected by L_2^* and L_3^*). The zero wave-number spectrum, one should remember, is equivalent to a volume integral of the stress.

The normal stress, u_1^2, is only responsible for radiation in the direction of the jet axis and not normal to it, but this does not effect the usefulness of the spectrum, $M_{1111}(\mathbf{y}, 0, \omega)$, as an approximation to those stress spectra which are responsible for radiation normal to the jet.

The acoustic spectra measured by Mollo-Christensen, Kolpin & Martuccelli (1964) are part of a most carefully performed experiment and the centre-line velocity of the jet, U_{CL}, is available in the results presented by Kolpin (1964). The acoustic spectrum has been calculated from (8.3), assuming the spectrum in figure 15 applies for all positions within the jet and using the centre-line velocity from Kolpin (1964) for an exit Mach number 0·8 and an exit diameter 1 in. This spectrum is compared in figure 17 with an arbitrary multiple of the acoustic spectrum at right angles to the jet measured by Mollo-Christensen *et al.* (1964). The 1 in. spectrum was chosen because the nozzle boundary layers were turbulent. The small nozzle examined by Mollo-Christensen *et al.* had laminar boundary layers and so is not well represented by the assumption that the stress intensity near the exit is proportional to U_{CL}. The measurements of Bradshaw (1966) in the region close to a nozzle with laminar boundary layers shows a region of very high turbulence downstream of the transition point. This region close to the exit will radiate sound of high frequency, and so possibly lead to an increase in the acoustic energy at these frequencies. This appears to be the case as the acoustic spectrum measured by Mollo-Christensen *et al.* (1964) on the 0·5 in. jet does have a greater proportion of energy at high frequency than the spectrum from the 1 in. jet.

9. Conclusions

The three turbulent intensities, $\sqrt{\overline{u_1^2}}/U_0$, $\sqrt{\overline{u_2^2}}/U_0$, $\sqrt{\overline{u_3^2}}/U_0$ in the two-dimensional jets were significantly different from each other in contrast with small round jets where the three intensities are approximately equal. The stress intensities, together with the stress length scales have been measured and should be useful for estimating the intensity of noise radiated.

In a jet, it seems that the four-dimensional stress correlation coefficient cannot be successfully separated in time *and* space. Thus measurements were made of frequency filtered signals to obtain the transform of the correlation rather than directly measuring the correlation itself. The difficulties in measuring the time differentiated stress correlation, needed for aerodynamic noise prediction, are considerable. If the stresses are time differentiated before measuring the correlation, the dominant components occur at very high frequencies where the correlations are small (outside the range of Strouhal number presented for the filtered length scales). These small length scales are difficult to measure accurately. If on the other hand the auto-correlation of the stress is measured and differentiated numerically, as Chu (1966) did, one has the difficulty of performing accurate numerical differentiation.

The agreement between the acoustic spectrum predicted with the aid of Lighthill's quadrupole theory from the turbulent stress measurements and the measured acoustic spectrum demonstrates the usefulness of turbulent stress measurements in understanding aerodynamic noise.

The author gratefully acknowledges the advice of Dr G. T. Csanady during the course of this work and the benefit of discussions with Mr P. Bradshaw concerning experimental techniques. This project has been supported financially by the Defence Research Board of Canada under a grant awarded to Dr G. T. Csanady.

REFERENCES

BRADSHAW, P. 1966 *J. Fluid Mech.* **26**, 225.

BRADSHAW, P., FERRISS, D. H. & JOHNSON, R. F. 1964 *J. Fluid Mech.* **19**, 591.

CHU, W. T. 1966 Univ. of Toronto, *UTIAS* Rep. no. 119.

DAVIES, P. O. A. L. & FISHER, M. J. 1963 *AGARD* Rep. no. 451.

FFOWCS WILLIAMS, J. E. 1963 *Phil. Trans.* A **255**, 469.

JONES, I. S. F. 1968 *J. Fluid Mech.* **33**, 65.

KOLPIN, M. A. 1964 *J. Fluid Mech.* **18**, 529.

LAUFER, J. 1955 *N.A.C.A.* Rep. no. 1174.

LIEPMANN, H. W. & LAUFER, J. 1947 *N.A.C.A.* Tech. Note 1257.

LIGHTHILL, M. J. 1952 *Proc. Roy. Soc.* A **211**, 564.

MOLLO-CHRISTENSEN, E., KOLPIN, M. A. & MARTUCCELLI, J. R. 1964 *J. Fluid Mech.* **18**, 285.

WILLS, J. A. B. 1964 *J. Fluid Mech.* **20**, 417.